# DISCLAIMER

This document was prepared as an account of work sponsored by the United States Government. While this document is believed to contain correct information, neither the United States Government nor any agency thereof, nor the Regents of the University of California, nor any of their employees, makes any warranty, express or implied, or assumes any legal responsibility for the accuracy, completeness, or usefulness of any information, apparatus, product, or process disclosed, or represents that its use would not infringe privately owned rights. Reference herein to any specific commercial product, process, or service by its trade name, trademark, manufacturer, or otherwise, does not necessarily constitute or imply its endorsement, recommendation, or favoring by the United States Government or any agency thereof, or the Regents of the University of California. The views and opinions of authors expressed herein do not necessarily state or reflect those of the United States Government or any agency thereof or the Regents of the University of California.

**Detachment of Liquid-Water Droplets from Gas-Diffusion Layers**

Prodip K. Das[a], Adam Grippin[a,b], and Adam Z. Weber[a]

[a] Lawrence Berkeley National Laboratory, 1 Cyclotron Road, Berkeley, CA 94720, USA

[b] Department of Chemical Engineering, University of Florida, Gainesville, FL 32611,

USA

A critical issue for optimal water management in proton-exchange-membrane fuel cells at lower temperatures is the removal of liquid water from the cell. This pathway is intimately linked with the phenomena of liquid-water droplet removal from surface of the gas-diffusion layer and into the flow channel. Thus, a good understanding of liquid-water transport and droplet growth and detachment from the gas-diffusion layer is critical. In this study, liquid-water droplet growth and detachment on the gas-diffusion layer surfaces are investigated experimentally to improve the understating of water transport through and removal from gas-diffusion layers. An experiment using a sliding-angle measurement is designed and used to quantify and directly measure the adhesion force for liquid-water droplets, and to understand the droplets' growth and detachment from the gas-diffusion layers.

**Introduction**

Proton-exchange-membrane fuel cells (PEMFCs) show great promise in becoming energy-delivery devices for a variety of future technologies, including stationary power generation and automotive applications. It is well known that water management is a critical component for successful PEMFC operation, especially at low operating temperatures and during startup/shutdown, where liquid-water is present (1-7). Water management is also critical for good PEMFC durability and lifetime because too little liquid-water can cause membrane dehydration and too much liquid-water can flood the cathode side of the PEMFC, causing less oxygen to reach the active catalyst sites and consequently decreasing the cell performance. Hence, a balanced liquid-water scheme is essential to achieve the full potential of a PEMFC. This scheme invariably involves the existence of liquid-water at some point during operation, and removal of it from the gas flow channel (GFC) becomes critically important. This removal is often through liquid-water droplets from the surface of the cathode gas-diffusion layer (GDL) and into the gas stream; understanding this process is essential. Therefore, the subject of liquid-water droplets' detachment from GDL surfaces is a fundamental problem for water transport in PEMFCs and its management. Droplet detachment from a surface is also important for various industrial and chemical processes, such as coating-flow manufacturing processes and enhanced oil recovery. To understand water transport through the GDL, liquid-water removal from the GDL surface, and transport throughout the PEMFC, mathematical and computational modeling has been utilized due to the complex nature of the materials and phenomena. Recently, several reviews have been published exploring the various models for GDL and PEMFC water management (8-12).

While much progress has been made in modeling of transport phenomena in PEMFCs, truly functional and predictive capabilities remain a challenge due to the lack of

fundamental understanding of liquid-water transport, particularly in the cathode catalyst layer and GDL. Most of the modeling approaches often rely on the empirical correlation between the liquid-water saturation and capillary pressure inside the GDL and neglect the liquid-water droplet growth and detachment from the GDL/GFC interface. Further, liquid-water saturation at the GDL/GFC interface is often considered negligible in the transport models of PEMFCs, while liquid-water droplets form continuously at the GDL/GFC interface. Therefore, the droplet growth and detachment from the GDL is not only vital for water management in the PEMFC but also critical for transport phenomena throughout the PEMFC.

A significant amount of experimental work devoted to the study of droplet dynamics in PEMFC flow channels has already highlighted some of the fundamental issues (13-15). Most of these studies, however, are based on contact-angle hysteresis of a stagnant droplet placed on top of a GDL. This hysteresis is defined as the difference between the advancing contact angle and the receding contact angle, $\theta_a - \theta_r$. An illustration of these angles is shown in Figure 1. Here, part (a) shows static contact angle ($\theta_c$) and surface tension forces for a liquid-water droplet on a typical PEMFC gas-diffusion surface, and part (b) shows advancing contact angle ($\theta_a$), receding contact angle ($\theta_r$) and sliding angle, ($\theta_s$). The sliding angle, also known as roll-off angle, indicates the angle of inclination of a surface when a droplet completely rolls off of the surface. The resistance force (known as adhesion force) that the droplet needs to overcome during the slide is shown in part (c).

The sliding angle, which is a measure of droplet mobility and detachment from a surface, is often estimated using a theoretical relation between the sliding angle and contact-angle hysteresis (16), although it was made clear that the contact-angle hysteresis

can only be a qualitative indication of drop mobility not a quantitative measure (17). Further, the advancing and receding contact angles measured on a level surface should theoretically not be used in predictions of sliding angles for a inclined surface (18). While the static contact angle and contact-angle hysteresis can provide insight on the liquid droplet movement on a solid surface, the correct identification of the contact angles at the edges of the drop can be extremely difficult on an inclined surface (19-21).

The dynamic behavior of water droplets is also strongly affected by the surface roughness, even on a scale of around 10 nm, and the history of the surface (22-24). Hence, the contact-angle hysteresis cannot be an index of dynamic hydrophobicity for liquid-water droplets on a porous PEMFC GDL, such as droplet motion or detachment, due to inherent surface roughness and complex structure of the GDL. Further, liquid-water in a PEMFC is transported from the catalyst layer to the GDL; hence, the pinning effect can have a strong influence on droplet movement along the GDL surface. It might be impossible to avoid a pinning effect for a droplet size of 1 mm or smaller, which is the typical droplet size for PEMFCs. Furthermore, contact-angle hysteresis does not provide an accurate estimation of the adhesion force between the liquid-water droplet and the GDL surface, while the adhesion force is the dominating force that is holding a liquid-water droplet on the GDL surface and preventing its detachment. Therefore, a direct measurement of sliding angle is the key to understanding liquid-water droplet movement and detachment from the PEMFC GDL.

In this study, we have designed and used a tilted-surface experiment to quantify and directly measure the sliding angles and adhesion force for liquid-water droplets on GDL surfaces. Our goal is to understand the fundamentals of liquid-water droplet formation,

adhesion and detachment from gas-diffusion surfaces through direct observation and measurements instead of static contact angle and its hysteresis.
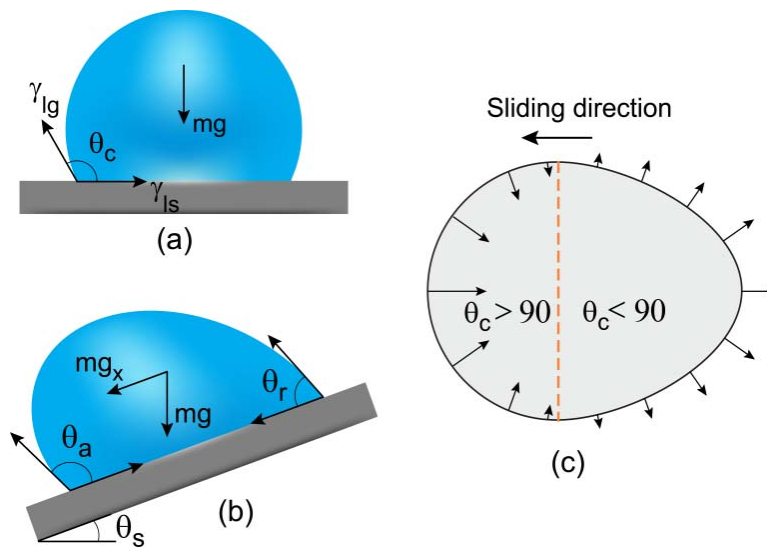


Figure 1. Illustration of contact angles and forces acting on a liquid-water droplet on a typical GDL surface. (a) Static contact angle ($\theta_c$) with the body force ($mg$) and surface tension forces ($\mu_{lg}$ and $\mu_{ls}$). (b) Advancing ($\theta_a$) and receding ($\theta_r$) contact angles and sliding (roll-off) angle ($\theta_s$). (c) Top view of the adhesion force distribution that is preventing the droplet from roll-off (parallel to the GDL surface); dashed line shows contact angle transition through 90°.

**Experimental**

The experimental measurements of sliding angles were performed using a modified automated Goniometer (ramé-hart Model 290) with a custom made injection system. The experimental setup with its key components is shown in Figure 2. A detailed description of the experimental apparatus and measurement procedure are given in the following paragraphs.

Apparatus

The liquid-water droplet profile images were taken using a CCD camera (70 fps) at 640×480 pixels for every half second; drops were backlit with a diffused 150 W halogen lamp. The camera was mounted to a stage that was inclined by a rotary motor at a constant angular speed of 1 or 0.5 °/s. Movement of the stage was vibration-free with no backlash and vibrations from surroundings were isolated from the stage using an anti-vibration stage to ensure that the liquid-water droplet does release due to gravity.

Injection methods and drop creation

Liquid-water droplets on SIGRACET carbon paper GDL (SGL Technologies GmbH, Meitingen, Germany) were placed using two injection methods (from the top and through the bottom of GDL sample) and two placement methods (placed on a horizontal surface and placed on a pre-tilted surface). For top injection, a porous GDL sample was attached with a solid substrate and then a fixed volume of liquid-water was injected using an automated dispensing system with a constant injection rate. The optimum injection rate was determined using several measurements. For smaller drops, it was found that the

sliding-angle data were statistically consistent for the injection rate of 2 µL/s. Therefore, a rate of 2 µL/s was used for the 5 µL droplets and for larger drops a rate of 1 µL/s was used, which ensures that the dynamic effect of droplet creation is minimal. Once a droplet reached the desired volume, the entire stage was inclined at a constant speed until the droplet completely rolled-off from the GDL surface.
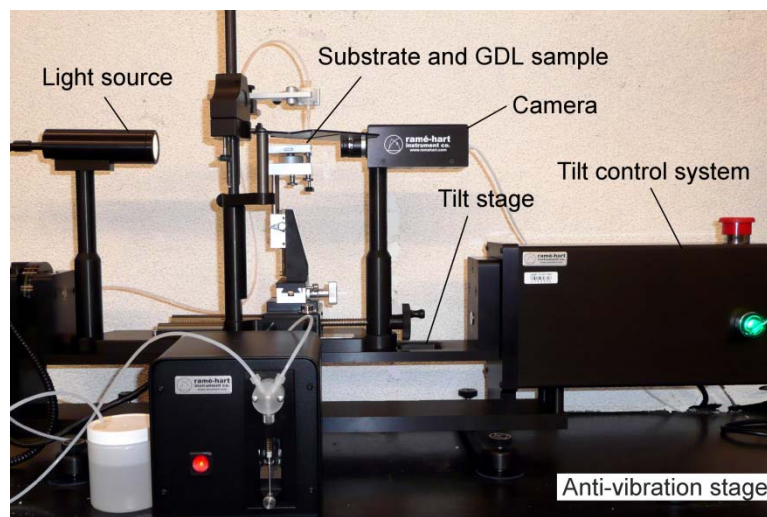


Figure 2. Setup used in the tilted-surface experiment to measure sliding angles and adhesion forces for GDL surfaces showing its key components.

It was observed that the addition of kinetic energy due to the angular motion of the stage is significant for a water droplet larger than 10 µL. For example, a 20 µL droplet on SGL 24DA (20 wt % polytetrafluoroethylene) GDL showed sliding angles of 4.62° and 6.62° for angular speeds of 1°/s and 0.5°/s, respectively. Conversely, a 5 µL droplet showed almost identical sliding angles for both speeds. Since the increase of droplet mass

is four times for a 20 μL droplet, the angular speed was reduced to half to minimize the addition of kinetic energy. Therefore, for smaller drops an angular speed of 1°/s and for larger drops an angular speed of 0.5°/s were used to reduce the effect of the stage's angular motion.

The bottom injection method was designed to mimic liquid-water transport process in a PEMFC cathode where liquid-water is produced in the catalyst layer and transported through the GDL, eventually appearing as droplets at the GDL/GFC interface. In this case, the GDL sample was attached with a pre-drilled solid-substrate to allow liquid-water to flow through the bottom of the GDL. Liquid-water was then injected through the bottom of the sample at a constant injection rate (between 0.25 to 1 μL/s) until the desired volume was reached. The injection speed was also critical to ensure the growth of only one droplet within the viewing window of the camera (~ 6 mm wide), as illustrated in Figure 3. As shown in Figure 3(a), multiple droplets formed and grew in a 6 mm wide region for an injection rate of about 20 μL/s, while at a lower injection rate multiple droplets were also formed but only one grew continuously as shown in Figure 3(b). Conversely, a controlled injection rate (usually 1 μL/s or less) always showed growth of only a single droplet as shown in Figure 3(c) and (d). Furthermore, the droplet volume and total injection volume were not equal for the bottom injection because of the porous nature of the GDL. The droplet volume was always less than the injection volume. Therefore, the volume of the droplet was first measured to ensure it reached the desired volume, and then the stage was inclined at a rate of 0.5°/s or 1°/s, depending on the droplet size, until the droplet completely rolled-off from the GDL surface.

(a) Fast injection

(b) Medium injection

(c) Slow and controlled injection

(d) Slow and controlled injection – droplet growth
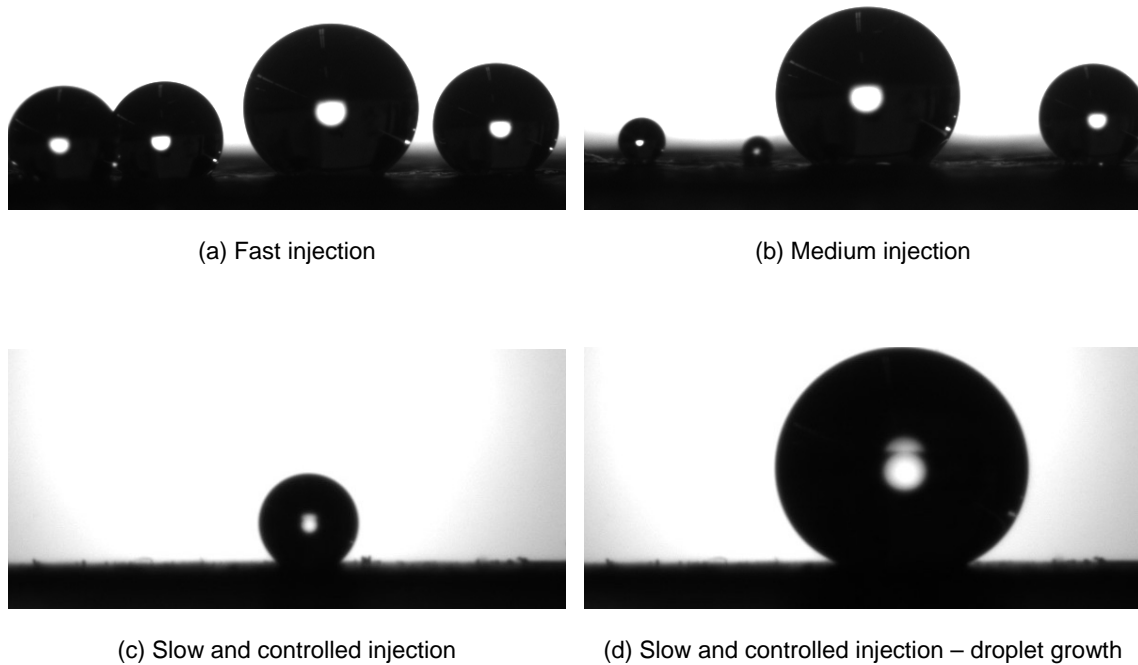
Figure 3. The effect of injection rate on the creation of liquid-water droplets on SGL 24 DA GDL for bottom injection method.

Placement methods

Two placement methods were used in this study, namely post-tilt and pre-tilt. In the post-tilt method, a liquid-water droplet was created on a horizontal surface using either top injection or bottom injection as described in the previous section, and then the stage was tilted at a constant speed until the droplet completely rolled-off from the GDL surface. Conversely, the entire stage was tilted to a desired angle of inclination before creating a droplet during the pre-tilt method. Liquid-water was then injected from the top or through the bottom of the sample at a constant injection rate until the droplet

completely rolled-off from the GDL surface. The effect of injection rate on droplet creation was significantly higher during the pre-tilt method. Therefore, a seed drop (usually less than 2 µL) was first grown on a horizontal GDL surface at a rate of 2 µL/s and liquid-water was then injected at a constant rate of 0.25 µL/s or higher until the droplet completely rolled-off from the GDL surface.

During the experiment, it was observed that precision is an issue of great concern with the sliding-angle measurements. Therefore, several measurements were taken for each data point to obtain statistically significant results. In order to increase the measurement confidence, eight to ten measurements were taken within 5% (or less) of the desired volume, and then the average and standard deviation of the sliding angles were calculated. Each measurement was entirely software controlled (DROPimage) and automated to ensure consistency for all the injection and placement methods.

## Results and Discussion

In the following sections, the results of the sliding-angle measurements using different methods are presented along with the estimated adhesion force between the liquid-water droplet and SGL 24DA gas-diffusion layer.

<u>Sliding angle measurement</u>

Figure 4 shows the measured sliding angles for liquid-water droplets on SGL 24DA for two injection methods, a top and a bottom injection. Here, the symbols represent the measured data with standard deviation, while the lines are the fitted curves. The correlations between the sliding angle and droplet volume for the top and bottom injection methods are

$$\theta_{s,t} = 22.547 e^{-0.077V}, \quad R^2 = 0.998 \tag{1}$$

and

$$\theta_{s,b} = 70.847 e^{-0.052V}, \quad R^2 = 0.995 \tag{2}$$

respectively, where $\theta_{s,t}$ and $\theta_{s,b}$ represent the sliding angles for top and bottom injection, respectively, and $V$ is the droplet volume in μL. Note that the sliding-angle data reported in this study represent complete roll-off from the GDL surface.

The static contact angles ($\theta_c$) for top and bottom injections for SGL 24DA GDL are found to be 151.05 ± 1.89° and 151.92 ± 6.04°, respectively. Although the injection methods do not show any significant effect on the static contact angle, the droplets placed using a bottom injection method have consistently higher sliding angles than those placed using a top injection method. This trend cannot be attributed to the addition of kinetic energy in the top injection method due to the large variation observed in Figure 4. It seems that the 'pinning' effect is significant for the bottom injection. Since liquid-water can flow through multiple pores of the GDL while injecting through the bottom of the GDL, liquid columns are formed underneath the droplet and assist the droplet's adhesion, and preventing it from detaching from the GDL surface. This situation results in a larger

wetted area (and wetted diameter) for a given droplet volume, and subsequently, larger

sliding angle as shown in Figure 4. The wetted diameter represents the diameter of the

contact area between the liquid-water droplet and the GDL surface. Furthermore, bottom

injection may create a thin liquid-water film on the GDL surface that can also assist the

droplet's adhesion and prevent sliding. Clearly, the results shown in Figure 4 indicate that

a GDL surface can exhibit higher adhesion forces depending on how the droplet is

formed. These results also elucidate why a static contact angle and its hysteresis are

inadequate for adhesion-force measurements.
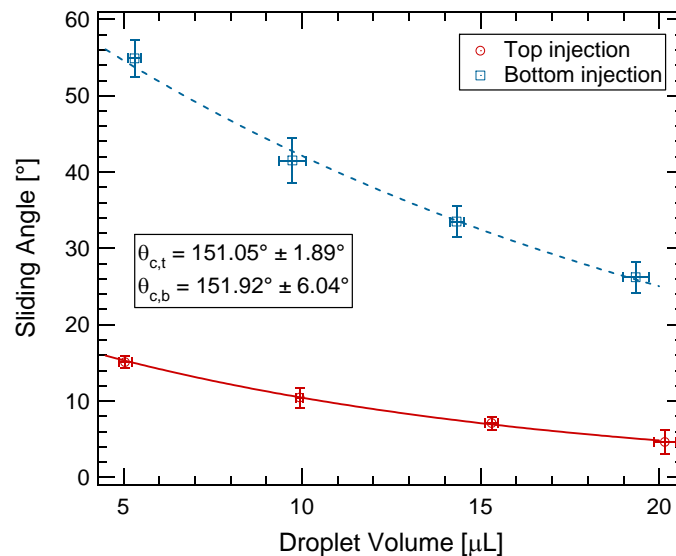


Figure 4. The dependence of the sliding angle on the injection method for SGL 24DA GDL. The symbols show the measured sliding angles for two injection methods as indicated in the legends, while the lines represent the fitted curves.

Figure 5 shows the measured volumes for liquid-water droplets on SGL 24DA for the pre-tilt method with bottom injection. Here, the symbols represent measured data with standard deviations for two GDLs (a used and an unused), while the line shows the sliding angles measured for droplets created on a horizontal unused-GDL surface (post-tilt method). For large droplets, the sliding angles are higher for droplets created on a horizontal surface than the droplets created on a pre-titled surface. For small droplets, the results show the opposite behavior, and the sliding angles are almost identical or higher for the pre-tilt method. A possible reason for this situation would be the addition of kinetic energy due to the injection rate in the pre-tilt method being higher. These data also illustrate that both the titled-surface (pre-tilt) and horizontal-surface (post-tilt) methods may adequately represent the physical problem of droplet growth and detachment from GDLs in PEMFCs when the droplets are smaller than 1 mm. The history of a GDL is also found to be important for sliding-angle measurements as a previously tested GDL (one day of use and left overnight uncovered) shows higher sliding angles than an untested GDL. The differences between the sliding-angle measurements are significant even with one day of use.
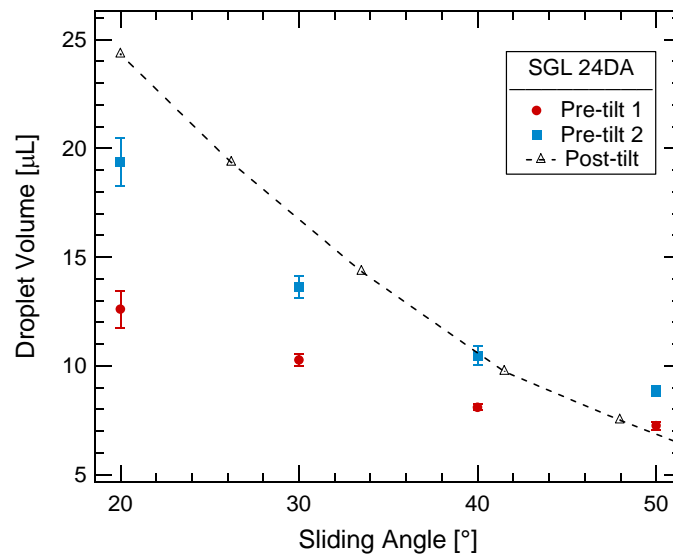
Figure 5. Measured droplet volume as a function of tilt angle for pre-tilt method with bottom injection. The symbols represent the pre-tilt data for an unused-GDL (pre-tilt 1) and a used-GDL (pre-tilt 2), while the dashed line depicts the data of post-tilt method with bottom injection for an unused SGL 24DA GDL.

Adhesion-force calculations

The adhesion force between the liquid-water droplet and GDL surface was calculated from the body force acting along the direction of slide and the wetted diameter. The measured wetted diameter of liquid-water droplets are shown in Figure 6 as a function of droplet volume for both top and bottom injection. As mentioned earlier, the wetted area (and wetted diameter) for a given drop volume is higher for bottom injection. Figure 6 provides evidence as to why bottom injection shows higher sliding angles, as observed in Figure 4. However, for smaller droplets, the wetted diameter is higher for top injection than the wetted diameter measured for bottom injection. This may be due to experimental error or the gravitational impact of the droplet on the GDL surface as it was higher for top injection no matter how low of injection rates were used.

The calculated adhesion forces between the liquid-water and SGL 24DA GDL are shown in Figure 7 as a function of droplet volume for both the top and bottom injection methods. As expected, the adhesion force (which is an intrinsic property) is independent of the droplet volume. The adhesion force between the liquid-water droplets and SGL

24DA are found to be 11.79 ± 0.23 N/m and 3.28 ± 0.10 N/m for bottom and top injection methods, respectively. The dependence of the adhesion force on injection method results in different droplet detachment criteria of the same surface in different application areas. Hence, it should not be assumed that the sliding angles are adequate to address the physical problem of droplet growth for every engineering application.
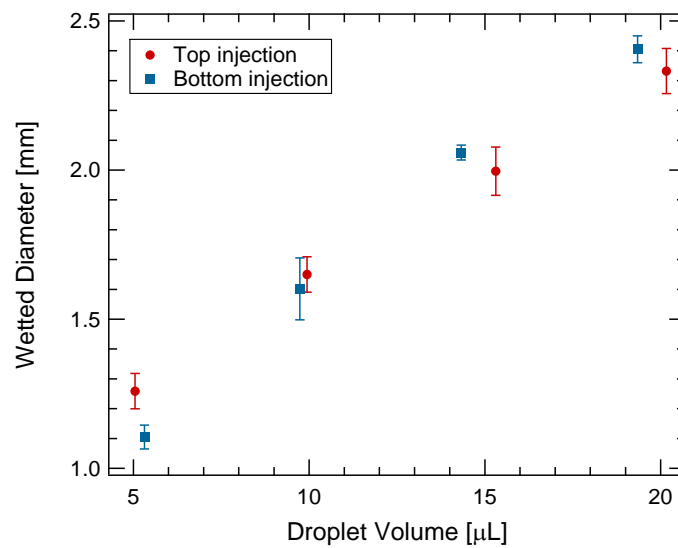


Figure 6. The dependence of the wetted diameter on the droplet volume for SGL 24DA GDL for top and bottom injections.
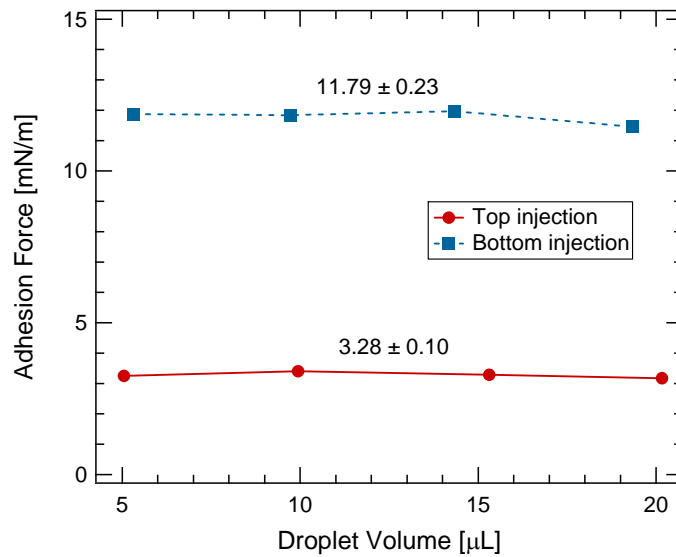
Figure 7. Adhesion forces between liquid-water droplets and SGL 24DA GDL for top and bottom injection methods.

## Concluding Remarks

In this study, an experimental protocol has been described for measuring directly the adhesion force for liquid-water droplets on a PEMFC GDL. It has been observed that both the droplet creation methods and the history of the GDL are equally important for droplet growth and detachment on a GDL surface. Furthermore, the top placement method commonly used is shown to underpredict the adhesion force in most cases compared to a water droplet generated by water moving through the GDL. The combination of contact-angle hysteresis and static contact angle seem to be inadequate to provide an accurate estimate of the adhesion force due to inherent pinning and dewetting effects, particularly for SGL 24DA or highly hydrophobic GDLs. Hence, the direct

measurement of sliding angles and adhesion forces are the only means to accurately predict droplet detachment and its instability on the GDL surface for PEMFCs.

## Acknowledgments

## References

1. D. M. Bernardi and M. W. Verbrugge, *AIChE J.*, **37**(8), 1151 (1991).

2. T. E. Springer, T. A. Zawodzinski and S. Gottesfeld, *J. Electrochem. Soc.*, **138**(8), 2334 (1991).

3. U. Pasaogullari and C. Y. Wang, *J. Electrochem. Soc.*, **151**(3), A399 (2004).

4. P. K. Sinha, P. P. Mukherjee and C. Y. Wang, *J. Mater. Chem.*, **17**(30), 3089 (2007).

5. P. K. Das, X. Li and Z. S. Liu, *Int. J. Hydrogen. Energ.*, **35**(6), 2403 (2010).

6. A. Z. Weber, *J. Power Sources*, **195**(16), 5292 (2010).

7. P. K. Das, X. Li, Z. Xie and Z. S. Liu, *Int. J. Energ. Res.*, (2011). DOI: 10.1002/er.1873.

8. C. Y. Wang, *Chem. Rev.*, **104**(10), 4727 (2004).

9. A. Z. Weber and J. Newman, *Chem. Rev.*, **104**(10), 4679 (2004).

10. N. Djilali, *Energy*, **32**, 269 (2007).

11. F. Barbir and S. Yazici, *Int. J. Energ. Res.*, **32**, 369 (2008).

12. K. Jiao and X. Li, *Prog. Energ. Combust.*, **37**(3), 221 (2011).

13. K. S. Chen, M. A. Hickner and D. R. Noble, *Int. J. Energ. Res.*, **29**(12), 1113 (2005).

14. E. C. Kumbur, K. V. Sharp and M. M. Mench, *J. Power Sources*, **161**(1), 333 (2006).

15. A. Theodorakakos, et al., *J. Colloid. Interf. Sci.*, **300**(2), 673 (2006).

16. C. G. Furmidge, *J. Coll. Sci.*, **17**(4), 309 (1962).

17. D. Oner and T. J. McCarthy, *Langmuir*, **16**(20), 7777 (2000).

18. B. Krasovitski and A. Marmur, *Langmuir*, **21**(9), 3881 (2005).

19. E. B. Dussan and R. T. P. Chow, *J. Fluid. Mech.*, **137**, 1 (1983).

20. E. B. Dussan, *J. Fluid. Mech.*, **174**, 381 (1987).

21. E. B. Dussan, *J. Fluid. Mech.*, **151**, 1 (1985).

22. M. Sakai, et al., *Surf. Sci.*, **600**(16), L204 (2006).

23. S. Suzuki, et al., *Appl. Surf. Sci.*, **254**(6), 1797 (2008).

24. T. Furuta, et al., *Langmuir*, **27**(11), 7307 (2011).